

# RSC Advances



This is an *Accepted Manuscript*, which has been through the Royal Society of Chemistry peer review process and has been accepted for publication.

*Accepted Manuscripts* are published online shortly after acceptance, before technical editing, formatting and proof reading. Using this free service, authors can make their results available to the community, in citable form, before we publish the edited article. This *Accepted Manuscript* will be replaced by the edited, formatted and paginated article as soon as this is available.

You can find more information about *Accepted Manuscripts* in the [Information for Authors](#).

Please note that technical editing may introduce minor changes to the text and/or graphics, which may alter content. The journal's standard [Terms & Conditions](#) and the [Ethical guidelines](#) still apply. In no event shall the Royal Society of Chemistry be held responsible for any errors or omissions in this *Accepted Manuscript* or any consequences arising from the use of any information it contains.

## Facile one-step mechanochemical synthesis of $[\text{Cu}(\text{tu})]\text{Cl}\cdot\frac{1}{2}\text{H}_2\text{O}$ nanobelts for high-performance supercapacitor

Di Guo, Hongxu Guo\*, Yingchang Ke, Dongfang Wang, Jianhua Chen,  
Qingxiang Wang, Wen Weng

College of Chemistry & Environmental, Minnan Normal University, Zhangzhou  
363000, P.R. China (E-mail to H. X. Guo: guohx@mnnu.edu.cn; Fax:  
086-596-2520035; Tel: 086-596-2591445)

### Abstract

A facile one-step mechanochemical process from  $\text{CuCl}_2\cdot 2\text{H}_2\text{O}$  and thiourea to fabricate novel  $[\text{Cu}(\text{tu})]\text{Cl}\cdot\frac{1}{2}\text{H}_2\text{O}$  nanobelts has been observed for the first time, and the nanobelts were used as an electrode material for a supercapacitor. The  $[\text{Cu}(\text{tu})]\text{Cl}\cdot\frac{1}{2}\text{H}_2\text{O}$  nanobelts with staggered arrangement have lengths longer than 10  $\mu\text{m}$ , and exactly straight nanobelts are 300 nm in width, and the extreme ends of nanobelts are around 30–50 nm in width. The specific capacitance of the  $[\text{Cu}(\text{tu})]\text{Cl}\cdot\frac{1}{2}\text{H}_2\text{O}$  nanobelts was up to 1145  $\text{F}\cdot\text{g}^{-1}$  at scan rate of 5  $\text{mV}\cdot\text{s}^{-1}$  and 922  $\text{F}\cdot\text{g}^{-1}$  at current density of 10  $\text{A}\cdot\text{g}^{-1}$  in a 2 M KOH electrolyte. Simultaneously, the retention was maintained at 72.4% after 500 cycles at 10  $\text{A}\cdot\text{g}^{-1}$ . The corresponding equivalent circuit for the  $[\text{Cu}(\text{tu})]\text{Cl}\cdot\frac{1}{2}\text{H}_2\text{O}$  was also discussed. This study provides a facile, green, and large-scale method to fabricate novel nano-complexes with high supercapacitor activity.

**Keywords:**  $[\text{Cu}(\text{tu})]\text{Cl}\cdot\frac{1}{2}\text{H}_2\text{O}$ ; Nanobelts; Mechanochemical synthesis; Energy storage and conversion; Nanocrystalline materials; Electrical properties

## 1. Introduction

The increasing demand for energy has emerged to be one of the major topics, alongside the energy storage and conversion from clean and renewable energy sources.

<sup>1</sup> Supercapacitors, also called electrochemical capacitors, are found to be promising for energy storage devices due to their high power densities, fast recharge capability and long cycle life.<sup>2</sup> Supercapacitors commonly store energy on the basis of either ion adsorption/desorption (electric double-layer capacitor, EDLCs) or multiple redox reactions (pseudocapacitors). The pseudocapacitors have a growing interest due to their higher energy densities than EDLCs and higher power densities than batteries.<sup>3</sup>

Combination of electrode materials,<sup>4</sup> including carbons,<sup>5</sup> metal oxides,<sup>6</sup> nitrides and polymers,<sup>7</sup> with the latest generation of coordination polymers have been explored for supercapacitors. Coordination polymers, as a class of hybrid materials built from metal ions and organic bridging ligands, have aroused tremendous interest because of their tunable structure and properties. Compared to conventional organic or inorganic nanomaterials, nanoscaled coordination polymers (NCPs) have been attracted more and more attention due to those interesting physical and chemical properties.<sup>8,9</sup> Recently, the application of the NCPs is mainly focused on sensors,<sup>10</sup> catalysis,<sup>11</sup> selective separation,<sup>12</sup> and optics.<sup>13</sup> The Ni-based MOFs exhibited a capacitance of  $668 \text{ F}\cdot\text{g}^{-1}$  at current density of  $10 \text{ A}\cdot\text{g}^{-1}$ .<sup>14</sup> And the most traditional methods for the preparation of coordination polymers was hydrothermal or solvothermal methods.<sup>15</sup>

In this paper we firstly report the facile and rapid synthesis of  $[\text{Cu}(\text{tu})]\text{Cl}\cdot 1/2\text{H}_2\text{O}$  nanobelts from  $\text{CuCl}_2\cdot 2\text{H}_2\text{O}$  and thiourea by a facile one-step mechanochemical method, and their application as electrode for supercapacitors with excellent energy storage properties. It should be noted that the mechanochemical synthesis is actually

faster and more convenient than the conventional solvent-based methods.<sup>16</sup> The as-prepared nanobelts exhibited high specific capacitance of  $1145 \text{ F}\cdot\text{g}^{-1}$  at scan rate of  $5 \text{ mV}\cdot\text{s}^{-1}$  and  $922 \text{ F}\cdot\text{g}^{-1}$  at current density of  $10 \text{ A}\cdot\text{g}^{-1}$  in a 2 M KOH electrolyte. Good rate capability and cycling performance that the retention was maintained at 72.4% after 500 cycles at  $10 \text{ A}\cdot\text{g}^{-1}$  were also demonstrated. This study provides a facile, green, and scale method to fabricate novel nano-complexes with high supercapacitor activity.

## 2. Experimental

All reagents in the experiment were analytical grade and used without further purification.  $[\text{Cu}(\text{tu})]\text{Cl}\cdot 1/2\text{H}_2\text{O}$  nanobelts was prepared by a facile green mechanochemical synthesis as follows: First of all, thiourea (0.7612 g, 10 mmol) were ground into powder. Then,  $\text{CuCl}_2\cdot 2\text{H}_2\text{O}$  (0.8524 g, 5 mmol) were ground together in a mortar for 20 minutes with sporadic drops of  $\text{C}_2\text{H}_5\text{OH}$  to keep reactants wet. The resulting solid was washed with  $\text{H}_2\text{O}$  to remove excess raw materials and dried at  $60 \text{ }^\circ\text{C}$  for 10 h. Light-green powders of as-prepared nanobelts were obtained (yield: 91%).

The as-prepared product was characterized with X-ray powder diffractometer (XRD, Bruker D8 Advance, Cu-K $\alpha$  radiation), fourier transform infrared spectroscopy (FTIR, Nicolet 6700), scanning electron microscopy (SEM, JEOL JSM-6010), transmission electron microscopy (TEM, FEI Tecnai G2 F20), thermo gravimetric (TG, Netzsch STA449F3), X-ray photoelectron spectroscopy (XPS, Thermo ESCALAB 250Xi). The specific surface area of sample was calculated by the Brunauere-Emmette-Teller (BET, Micrometrics GEMINI VII 2390) equation.

The electrochemical properties were measured using a potentiostat (CHI660E,

Shanghai Chenhua Limited, China) based on a conventional three-electrode system consisted of the working electrode, a platinum as the counter electrode, and a saturated calomel electrode as the reference electrode in a 2 M KOH electrolyte. The working electrode was prepared by mixing  $[\text{Cu}(\text{tu})]\text{Cl}\cdot\frac{1}{2}\text{H}_2\text{O}$  nanobelts (80 wt%) as active material with acetylene black (10 wt%), and poly(tetrafluoroethylene) (10 wt%). Then, the resulting mixture with several drops of ethanol was coated onto a piece of nickel foam (1.0 cm $\times$ 1.0 cm) using a spatula. Finally, the fabricated electrode was pressed at 2 MPa to a thin foil and then dried under vacuum at 60 °C for 10 h. The mass loading of the sample was about  $\sim$ 2 mg. EIS data was performed with a frequency range from 0.1 Hz to 100 kHz at open-circuit potential. The amplitude of the applied sine wave potential in each case was 5 mV.

### 3. Results and discussion

The crystal structure of the  $[\text{Cu}(\text{tu})]\text{Cl}\cdot\frac{1}{2}\text{H}_2\text{O}$  nanobelts was determined by XRD. It can be seen from Fig. 1 that the diffraction pattern in this pattern can be indexed to be the monoclinic phase of  $[\text{Cu}(\text{tu})]\text{Cl}\cdot\frac{1}{2}\text{H}_2\text{O}$  (JCPDS No. 53-0121) from the reference document.<sup>17,18</sup> The strong and sharp diffraction peaks in the XRD pattern indicated that the product was well crystallized. And the main peak of the  $[\text{Cu}(\text{tu})]\text{Cl}\cdot\frac{1}{2}\text{H}_2\text{O}$  nanobelts was located at 8.2°, corresponding to its polymeric nature.

The FTIR spectra (Fig. 2) of  $[\text{Cu}(\text{tu})]\text{Cl}\cdot\frac{1}{2}\text{H}_2\text{O}$  nanobelts and thiourea exhibited vibrational bands in the usual region of 400–4000  $\text{cm}^{-1}$ . It can be seen clearly that the main characteristic peaks in thiourea molecular were also observed in the  $[\text{Cu}(\text{tu})]\text{Cl}\cdot\frac{1}{2}\text{H}_2\text{O}$  compound. The bands at of 3500–3000,  $\sim$ 1600,  $\sim$ 1400 and

1300-1000  $\text{cm}^{-1}$  were ascribed to the stretching vibration of N–H, the bending vibrations of N–H, the stretching vibration of C–N and C=S, respectively.<sup>17</sup> And the split peak at 1658  $\text{cm}^{-1}$  of the  $[\text{Cu}(\text{tu})]\text{Cl}\cdot 1/2\text{H}_2\text{O}$  nanobelts was ascribed to the bending vibration of the crystallized  $\text{H}_2\text{O}$ . The peak at 1085  $\text{cm}^{-1}$  of C=S vibrational mode was found in thiourea, while the peak of the C=S vibrational mode was located at 1053  $\text{cm}^{-1}$  in the  $[\text{Cu}(\text{tu})]\text{Cl}\cdot 1/2\text{H}_2\text{O}$  nanobelts, which thus red shift in the bands suggests that the Cu-S bond formed in the compound. The peak at 750  $\text{cm}^{-1}$  was attributed to the bond Cu-S.<sup>10</sup>

The morphology and nanostructure of the  $[\text{Cu}(\text{tu})]\text{Cl}\cdot 1/2\text{H}_2\text{O}$  nanobelts was investigated by SEM and TEM. The SEM image Fig. 3a depicts that the  $[\text{Cu}(\text{tu})]\text{Cl}\cdot 1/2\text{H}_2\text{O}$  nanobelts have lengths longer than 10  $\mu\text{m}$ . Fig. 3b shows a high-magnification SEM image of the intertwined nanobelts with approximate dimensions of 300 nm in width. But, the extreme ends of nanobelts are around 30–50 nm in width, and the smooth surface and uniform diameter of each nanobelts along its entire length indicates its complete growing and ordered array of the structure, as shown in Fig. 3c and 3d.

The thermal study of the  $[\text{Cu}(\text{tu})]\text{Cl}\cdot 1/2\text{H}_2\text{O}$  nanobelts was performed in Fig. 4. The first small weight loss at 50~150  $^{\circ}\text{C}$ , corresponded to the removal of water and solvent molecules. The  $[\text{Cu}(\text{tu})]\text{Cl}\cdot 1/2\text{H}_2\text{O}$  nanobelts showed 45% decreased weight loss at 162~322  $^{\circ}\text{C}$ , which indicating the elimination of thiourea of  $[\text{Cu}(\text{tu})]\text{Cl}\cdot 1/2\text{H}_2\text{O}$  nanobelts. A mass loss (18%) from 380 to 800  $^{\circ}\text{C}$  was observed, which was assigned to the thermal decomposition of the chlorine and framework. And the final residue was copper under the atmosphere of  $\text{N}_2$ .<sup>10</sup>

The surface chemical composition and chemical states of the samples studied

were investigated by XPS. The XPS spectra of the [Cu(tu)]Cl•1/2H<sub>2</sub>O nanobelts sample are shown in Fig. 5. The obvious peaks of Cu, S, Cl, C and N can be clearly detected in the survey spectrum of the sample (Fig. 5a). The C 1s signal on [Cu(tu)]Cl•1/2H<sub>2</sub>O nanobelts (Fig. 5b) was fitted by three peaks, where the peaks at 288.6 and 287.8 eV were attributed to the organic carbon.<sup>19</sup> and the other one at 284.8 eV was attributed to the sp<sup>3</sup> C–C bond.<sup>20</sup> For the N 1s signal as shown in Fig. 5c, three fitted peaks in [Cu(tu)]Cl•1/2H<sub>2</sub>O nanobelts was assigned to N–C (400.1 eV), C–H (399.5 eV).<sup>21,22</sup> The Cl 2p XPS spectrum (Fig. 5d) can be deconvoluted into three different signals with binding energies of 199.4, 198.1, and 197.6 eV, corresponding to Cl 2p<sub>3/2</sub>, the Cl 2p<sub>3/2</sub> coordinated with copper, and Cl 2p<sub>1/2</sub>, respectively.<sup>23,24</sup> In the XPS S 2p spectra (Fig. 5e), the deconvoluted doublet peaks located at the binding energy of 164.0 eV (S 2p<sub>1/2</sub>) and 162.7 eV (S 2p<sub>3/2</sub>) are characteristic of S<sup>2-</sup>.<sup>25</sup> Fig. 5f showed the XPS spectra of Cu 2p for [Cu(tu)]Cl•1/2H<sub>2</sub>O nanobelts. It was notable that there were two strong peaks around 952.3 and 932.3 eV, which can be indexed to the Cu 2p<sub>1/2</sub> and Cu 2p<sub>3/2</sub> energy positions of the Cu(I) species with different coordination.<sup>26</sup>

The N<sub>2</sub> adsorption–desorption measurement was performed to investigate the textural characteristics of the [Cu(tu)]Cl•1/2H<sub>2</sub>O nanobelts in Fig. 6. It was found that the isotherms belonged to a type II corresponding to the basic no pores. An H3-type hysteresis loop at high relative pressure reflected the formation of slit-shaped pores from aggregates of nanobelts.<sup>27</sup> And the porosity of the [Cu(tu)]Cl•1/2H<sub>2</sub>O nanobelts was calculated by Barret–Joyner–Halenda (BJH) method, which revealed the five most probable pore diameters of 44.3 nm, 62.5 nm, 83.2 nm, 119.9 nm and 541.5 nm, respectively (Fig. 6, inset).

The electrochemical properties of the [Cu(tu)]Cl•1/2H<sub>2</sub>O nanobelts as an integrated electrode were investigated first in the three-electrode configuration with 2 M KOH as the electrolyte. As shown in Fig. 7a, CV profiles were obtained for the voltage sweeps from -0.2 to 0.8 with a series of scan rates from 5 to 100 mV•s<sup>-1</sup>, which delivered the capacitance of 1145, 974, 826, 657 and 536 F•g<sup>-1</sup> at scan rates of 5, 10, 20, 50 and 100 mV•s<sup>-1</sup>, respectively. Clearly, the emergence of one pair of the well-defined redox peaks (-0.05 V and 0.58 V) for the [Cu(tu)]Cl•1/2H<sub>2</sub>O sample can be observed. And the formation of the redox peaks was probably attributed to the faradaic redox reactions between the electrode material and the alkaline electrolyte. Moreover, with the increase of scan rate, the anodic peaks shifted to positive potential while the cathodic peaks shifted to negative potential, which may be originated from the faster charge and discharge rates and the short ion diffusion path.<sup>28</sup> This can be proved by the fact that the [Cu(tu)]Cl•1/2H<sub>2</sub>O sample is good electrode materials for pseudocapacitors, which undergo redox reactions simultaneously with OH<sup>-</sup>, hence contributing to the capacitance enhancement of pseudocapacitors. The corresponding process of Cu<sup>+</sup>/Cu<sup>2+</sup> transition might be represented by the following equation:<sup>14,29</sup>



The galvanostatic charge discharge curves of the [Cu(tu)]Cl•1/2H<sub>2</sub>O nanobelts electrode showed symmetric and reversible charge-discharge processes even at high current densities, which was indicative of efficient pseudocapacitor formation, as shown in Fig. 7b. From the discharge curve, the specific capacitance was calculated as 922, 766, 702, 662, 630 and 602 F•g<sup>-1</sup> at current densities of 10, 14, 18, 22, 26 and 30 A•g<sup>-1</sup>, respectively.

The EIS spectra, a magnified view of the high-frequency region and the corresponding equivalent circuit were carried out in Fig. 7c. At the high frequency, the below zero part of the curve at the real part indicated the inductive reactance ( $L$ , which was equivalent to inductive component, was related to electrode wire) and the intersection reflected the low equivalent series resistance ( $R_s = 0.88 \Omega$ , which included the inherent resistance of the electroactive material, the ionic resistance of electrolyte, and the contact resistance at the interface between electrode and electrolyte).<sup>29</sup> This low value showed the excellent electrical conductivity for the as-prepared sample. Moreover, the semicircular loop in the high-frequency region which associated with electrode surface properties and related to the charge-transfer resistance ( $R_{ct}$ ) was negligible in the inset. At the low frequency, the Nyquist impedance plot exhibited a sloped line which represented the diffusive resistance ( $W$ ), indicating the fast diffusion process of ions.<sup>30-34</sup>

The good electrochemical performance of the  $[\text{Cu}(\text{tu})]\text{Cl}\cdot\frac{1}{2}\text{H}_2\text{O}$  nanobelts was further confirmed by the cycling test at  $10 \text{ A}\cdot\text{g}^{-1}$  (Fig. 7d). After 500 cycles, the  $[\text{Cu}(\text{tu})]\text{Cl}\cdot\frac{1}{2}\text{H}_2\text{O}$  nanobelts was also capable of retaining 72.4% of the initial capacitance.

#### 4. Conclusions

In summary, a facile one-step mechanochemical process to fabricate  $[\text{Cu}(\text{tu})]\text{Cl}\cdot\frac{1}{2}\text{H}_2\text{O}$  nanobelts has been observed for the first time, and the nanobelts were used as an electrode material for a supercapacitor. The specific capacitance of the  $[\text{Cu}(\text{tu})]\text{Cl}\cdot\frac{1}{2}\text{H}_2\text{O}$  nanobelts was up to  $922 \text{ F}\cdot\text{g}^{-1}$  at current density of  $10 \text{ A}\cdot\text{g}^{-1}$  in a 2 M KOH electrolyte. Simultaneously, the retention was maintained at 72.4% after 500 cycles at  $10 \text{ A}\cdot\text{g}^{-1}$ . This study provides a facile, green, and large-scale method to

fabricate novel nano-complexes with high supercapacitor activity.

## References

- 1 Y. Gogotsi and P. Simon, *Science*, 2011, 334, 917.
- 2 J. R. Miller and P. Simon, *Science*, 2008, 321, 651.
- 3 H. Huo, Y. Zhao and C. Xu, *J. Mater. Chem. A*, 2014, 2, 15111.
- 4 P. Simon and Y. Gogotsi, *Nat. Mater.*, 2008, 7, 845.
- 5 M. J. Zhi, C. C. Xiang, J. T. Li, M. Li and N. Q. Wu, *Nanoscale*, 2013, 5, 72.
- 6 Y. B. He, G. R. Li, Z. L. Wang, C. Y. Su and Y. X. Tong, *Energ. Environ. Sci.*, 2011, 4, 1288.
- 7 H. Jiang, J. Ma and C. Z. Li, *J. Mater. Chem.*, 2012, 22, 16939.
- 8 A. M. Spokoyny, D. Kim, A. Sumrein and C. A. Mirkin, *Chem. Soc. Rev.*, 2009, 38, 1218.
- 9 M. Y. Masoomi and A. Morsali, *Coordin. Chem. Rev.*, 2012, 256, 2921.
- 10 S. Sarkar, S. Dutta, S. Chakrabarti, P. Bairi and T. Pal, *ACS Appl. Mater. Inter.*, 2014, 6, 6308.
- 11 Y. Liao, L. He, J. Huang, J. Zhang, L. Zhuang, H. Shen and C. Su, *ACS Appl. Mater. Inter.*, 2010, 2, 2333.
- 12 M. Paul, N. N. Adarsh and P. Dastidar, *Cryst. Growth Des.*, 2012, 12, 4135.
- 13 F. Fleischhaker, A. C. Arsenault, V. Kitaev, F. C. Peiris, G. V. Freymann, I. Manners, R. Zentel and G. A. Ozin, *J. Am. Chem. Soc.*, 2005, 127, 9318.
- 14 J. Yang, P. Xiong, C. Zheng, H. Qiu and M. Wei, *J. Mater. Chem. A*, 2014, 2, 16640.
- 15 K. M. Choi, H. M. Jeong, J. H. Park, Y. Zhang, J. K. Kang and O. M. Yaghi, *ACS nano.*, 2014, 8, 7451.

- 16 T. Friscic, *J. Mater. Chem.*, 2010, 20, 7599.
- 17 J. Mao, Q. Shu, Y. Wen, H. Yuan, D. Xiao and M. M. F. Choi, *Cryst. Growth & Des.*, 2009, 9, 2566.
- 18 Z. Fang, C. Wang, F. Fan, S. Hao, L. Long, Y. Song and T. Qiang, *Chin. J. Chem.*, 2013, 31, 1015.
- 19 P. V. Lakshminarayanan, H. Toghiani and C. U. Pittman Jr, *Carbon*, 2004, 42, 2433.
- 20 S. Martha, A. Nashim and K. M. Parida, *J. Mater. Chem. A.*, 2013, 1, 7816.
- 21 J. S. Stevens, S. J. Byard, C. C. Seaton, G. Sadiq, R. J. Davey and S. L. M. Schroeder, *Phys. Chem. Chem. Phys.*, 2014, 16, 1150.
- 22 J. M. L. Martínez, E. R. Castellón, R. M. T. Sánchez, L. R. Denaday, G. Y. Buldain and V. C. Dall'Orto, *J. Mol. Catal. A-Chem.*, 2011, 339, 43.
- 23 J. H. Carrillo, A. Marinas, J. M. Marinas, J. J. Delgado, R. R. Miranda and F. J. Urbano, *Appl. Catal. B-Environ.*, 2014, 154, 369.
- 24 L. Han, P. Hu, Z. Xu and S. Dong, *Electrochim. Acta.*, 2014, 115, 263.
- 25 C. Nethravathi, A. A. Jeffery, M. Rajamathi, N. Kawamoto, R. Tenne, D. Golberg and Y. Bando, *ACS nano.*, 2013, 7, 7311.
- 26 R. Zhao, T. Yang, M. A. Miller and C. K. Chan, *Nano Lett.*, 2013, 13, 6055.
- 27 Z. Liu, X. Tan, X. Gao and L. Song, *J. Power Sources*, 2014, 267, 812.
- 28 L. Mai, F. Yang, Y. Zhao, X. Xu, L. Xu and Y. Luo, *Nat. Commun.*, 2011, 2, 381.
- 29 C. Zhou, Y. Zhang, Y. Li and J. Liu, *Nano Lett.*, 2013, 13, 2078.
- 30 J. Wang, S. Wang, Z. Huang and Yaming Yu, *J. Mater. Chem. A*, 2014, 2, 17595.
- 31 F. Wan, X. Wu, J. Guo, J. Li, J. Zhang, L. Niu and R. Wang, *Nano Energy*, 2015, 13, 450.
- 32 X. Wu, Y. Guo, J. Su, J. Xiong, Y. Zhang and L. Wan, *Adv. Energy Mater.*, 2013,

3, 1155.

33 W. Li, H. Lü, X. Wu, H. Guan, Y. Wang, F. Wan, G. Wang, L. Yan, H. Xie and R.

Wang, *RSC Adv.*, 2015, 5, 12583.

34 X. Wu, W. Wang, Y. Guo and L. Wan, *J. Nanosci. Nanotechnol.*, 2011, 11, 1897.

### **Acknowledgement**

This work was supported by the Science and technology key project of Fujian (2013H0053), the Nature Science Foundation of Fujian (2012J06005), the key laboratory of urban environment and health, institute of urban environment, Chinese Academy of Sciences (KLUEH201305) and fund of innovation team from Minnan Normal University.

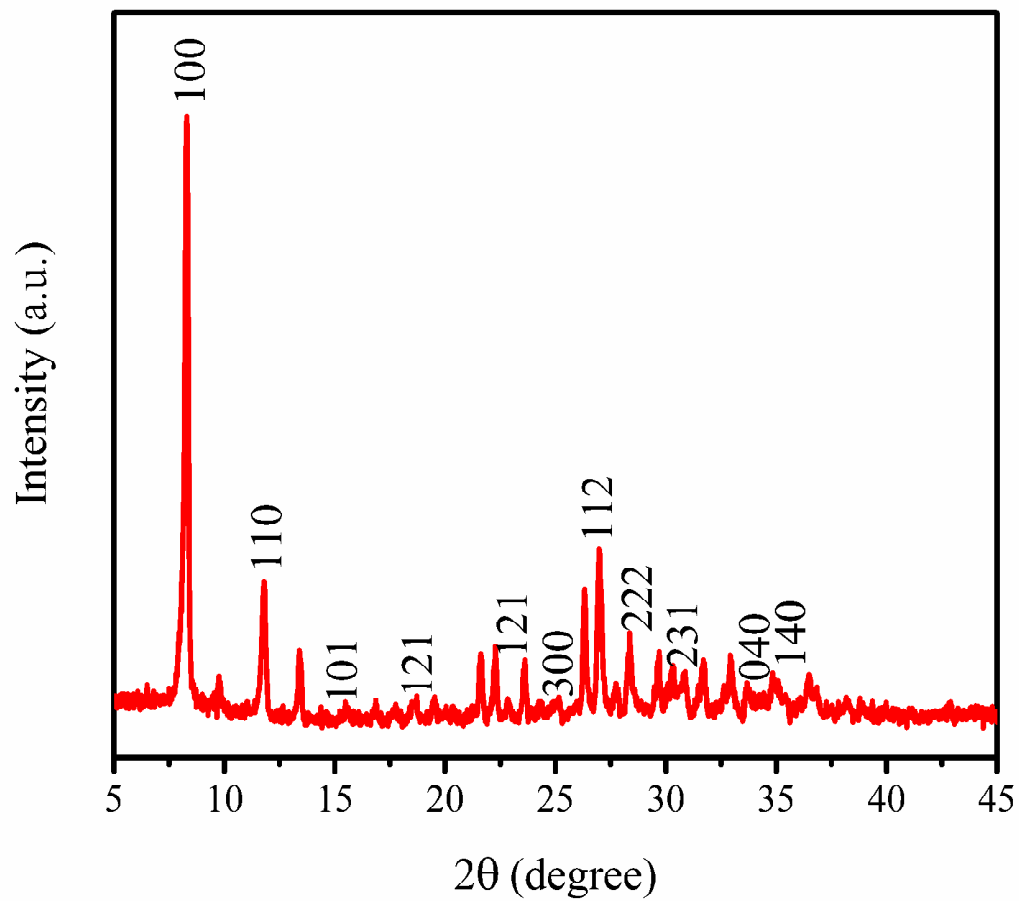


Fig. 1. XRD pattern of as-prepared [Cu(tu)]Cl·1/2H<sub>2</sub>O nanobelts.

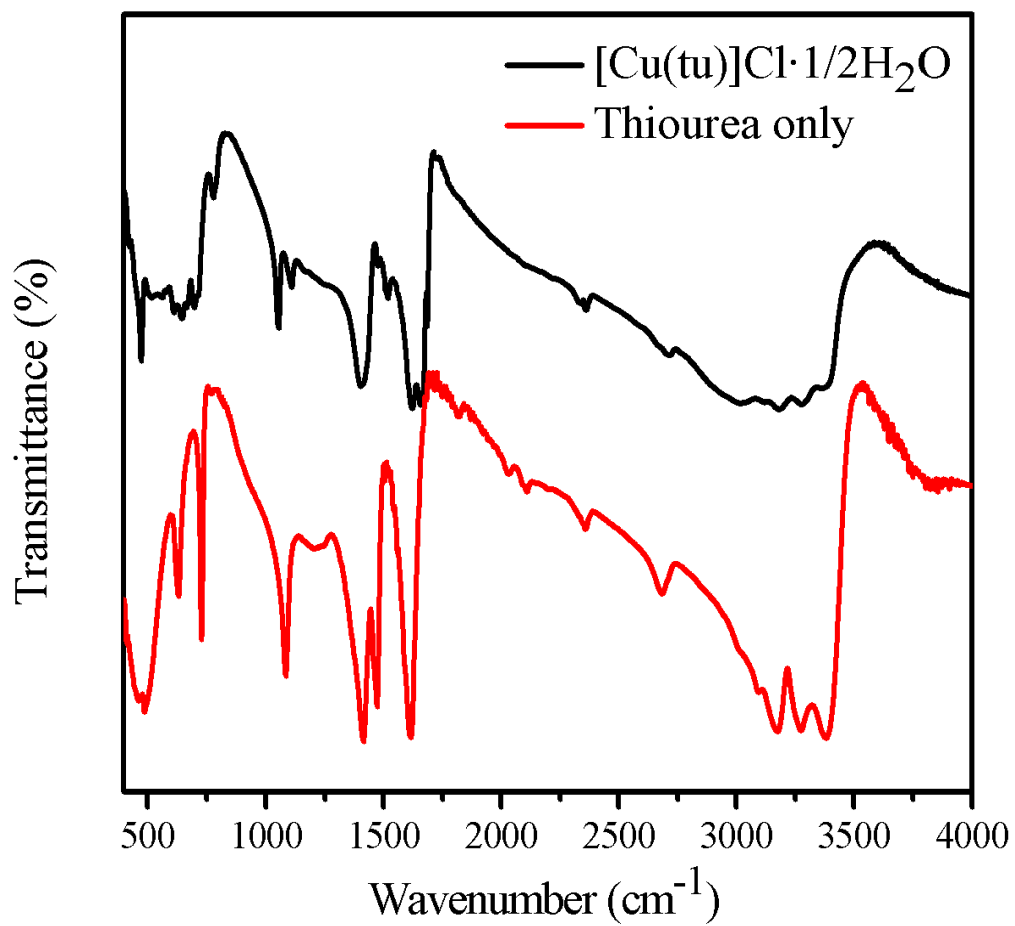


Fig. 2. IR spectra of [Cu(tu)]Cl·1/2H<sub>2</sub>O nanobelts and thiourea.

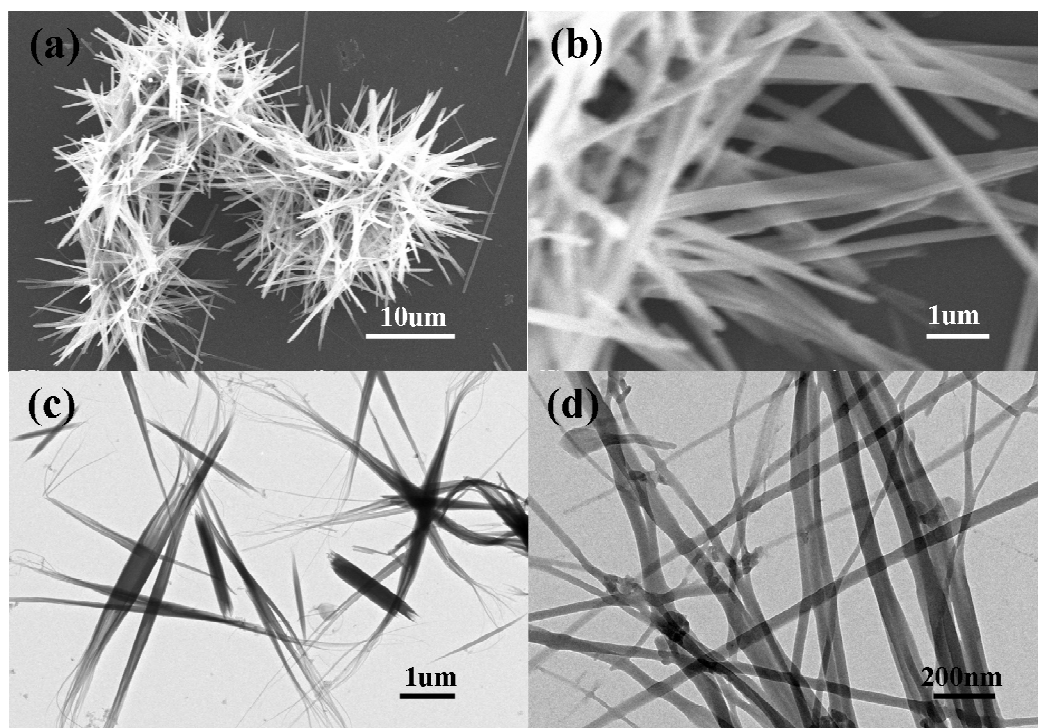


Fig. 3. SEM images (a and b), TEM images(c and d) of [Cu(tu)]Cl·1/2H<sub>2</sub>O nanobelts.

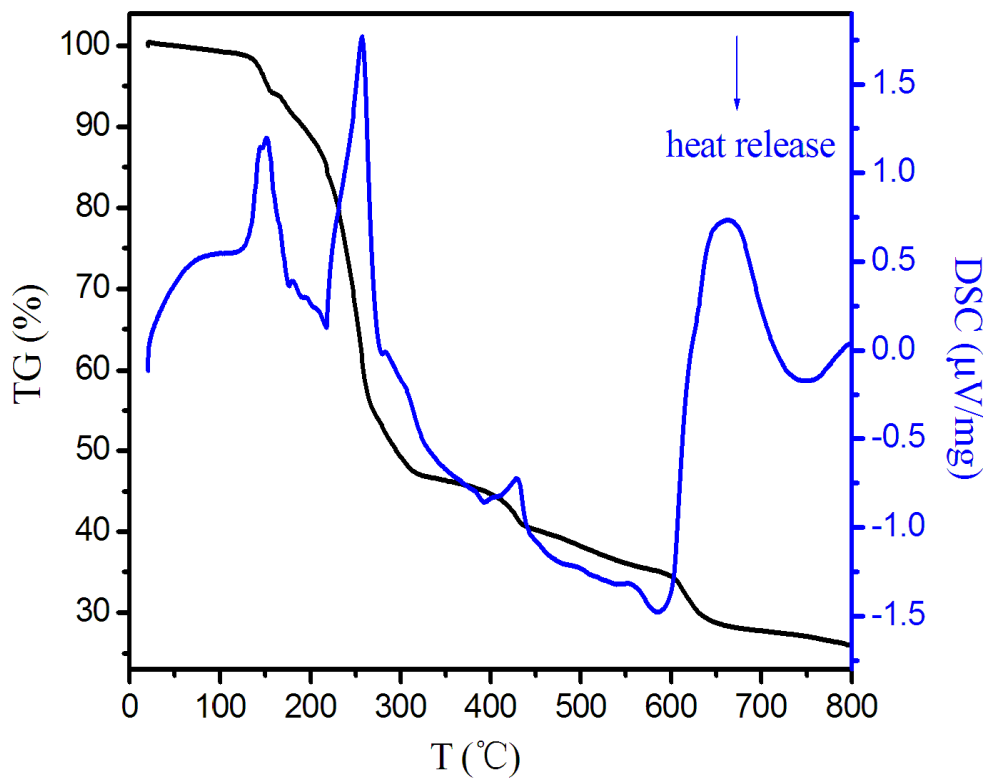


Fig. 4. TGA of  $[\text{Cu}(\text{tu})]\text{Cl}\cdot\frac{1}{2}\text{H}_2\text{O}$  nanobelts.

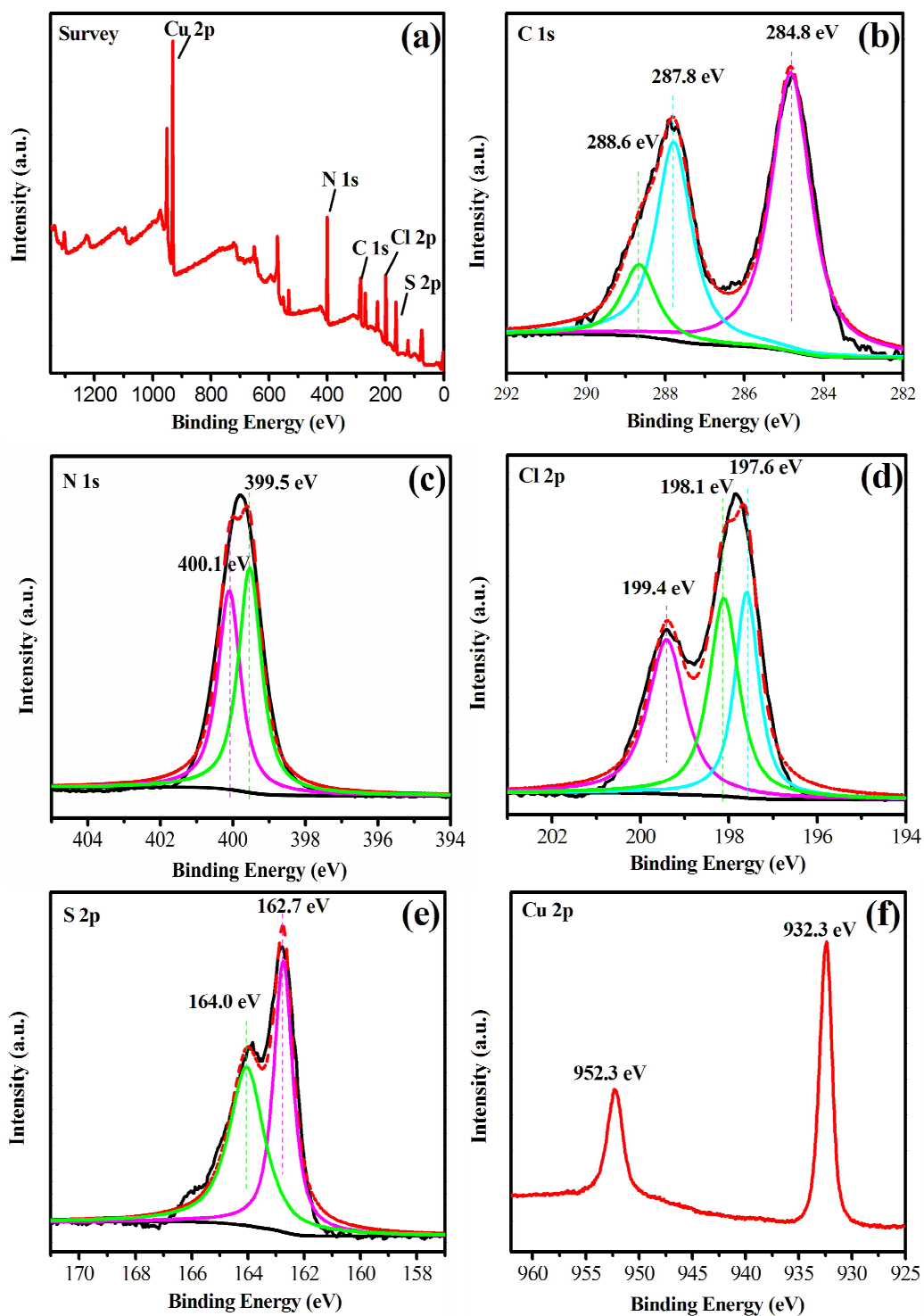


Fig. 5. XPS spectra of [Cu(tu)]Cl·1/2H<sub>2</sub>O nanobelts: (a) the survey scan; (b) C 1s; (c) N 1s; (d) Cl 2p; (e) S 2p; and (f) Cu 2p.

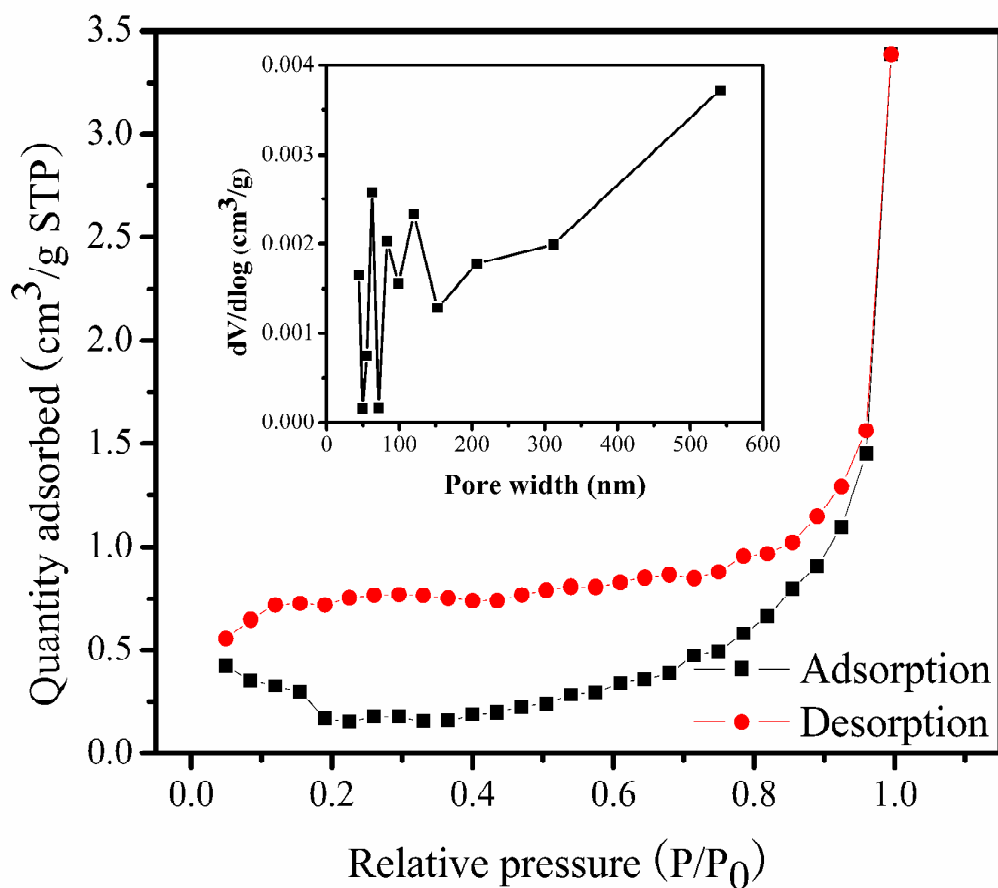


Fig. 6. N<sub>2</sub> adsorption–desorption isotherms of [Cu(tu)]Cl·1/2H<sub>2</sub>O nanobelts measured at 77 K. Inset shows the BJH mesoporous size distribution plots.

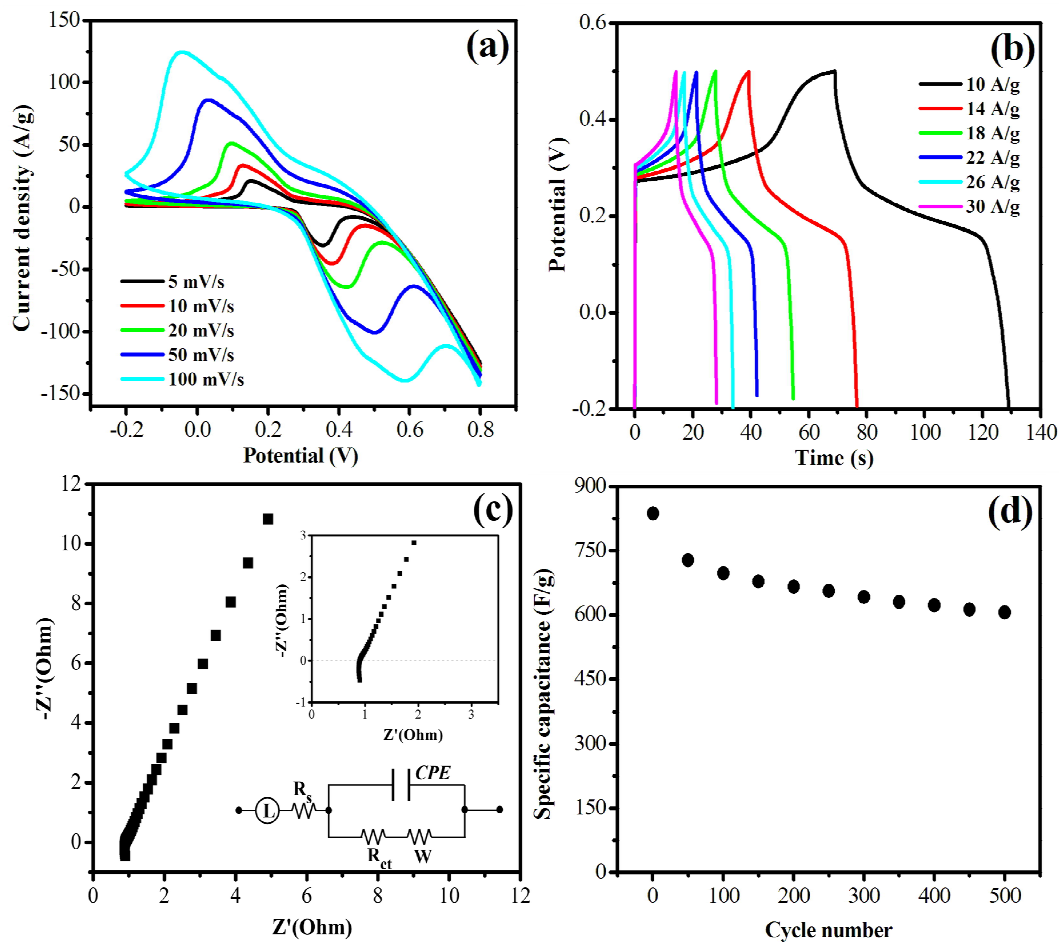


Fig. 7. Electrochemical characterization of [Cu(tu)]Cl·1/2H<sub>2</sub>O nanobelts. (a) Cyclic voltammetry curves; (b) galvanostatic charge discharge curves; (c) Nyquist plot and the inset showed the magnifies data and the corresponding equivalent circuit; (d) cycling stability performance.